Available online at www.sciencedirect.com
SCIENCE DIRECT®
Journal of Power Sources 134 (2004) 185–196
JOURNAL OF POWER SOURCES
www.elsevier.com/locate/jpowsour

Performance studies of PEM fuel cells with interdigitated flow fields

Lin Wang, Hongtan Liu*
Department of Mechanical Engineering, University of Miami, Coral Gables, FL 33146, USA

Received 8 March 2004; accepted 28 March 2004
Available online 17 June 2004

Abstract

Efforts in developing various models for PEM fuel cells have been increasing in recent years, and thus creating an urgent need for systematic experimental data on fuel cells with commercially available components. Such systematic experimental data is also needed by new fuel cell developers to accelerate their system development and optimization. To meet these needs, we present in this paper systematic experimental data on the performance of a proton exchange membrane fuel cell with interdigitated flow fields. The experiments concentrate on the effects of cell temperature, gas humidification, cell operating pressure and reactant gas flow rate. The experimental results are presented in the form of polarization curves. In addition, a three-dimensional fuel cell mathematical model is used to simulate the cell performance with the interdigitated flow fields. The comparison of the modeling results and experimental data shows a good agreement.

Keywords: Interdigitated flow field; PEM fuel cells; Fuel cells

1. Introduction

For most proton exchange membrane (PEM) fuel cell designs, reactant gases are fed into the fuel cell through the gas flow fields grooved on the collector plates. There are different designs of gas flow fields. The traditional design is the serpentine flow field, which is shown in Fig. 1(a). With this type of flow field, the reactant gases are transported from the gas channels to the catalyst layers mainly by diffusion. While with the interdigitated flow field, the transport mechanisms are not only diffusion but also forced convection, thus enhancing the mass transfer of reactant gases. The diagram of an interdigitated flow field is shown in Fig. 1(b).

We have presented a parametric study on PEM fuel cells with the serpentine flow field [1], but very limited experimental studies on interdigitated flow fields have been published. Nguyen [2] presented a comparative experimental study on a fuel cells with interdigitated flow fields and parallel straight channel flow fields, which showed that the fuel cell with the interdigitated flow fields outperformed the cell with the parallel straight channel flow fields. Wood et al. [3] studied the effect of direct liquid water injection on the performance of PEM fuel cells with interdigitated flow fields.

Some mathematical models were developed to study the performance of PEM fuel cells with interdigitated flow fields. Kazim et al. [4] developed a simple two-dimensional mathematical model and used the model to compare the performance of a fuel cell with parallel straight channel flow fields and interdigitated flow fields. This study showed that the limit current density increased threefold and the maximum power doubled when the interdigitated flow fields were used. Yi and Nguyen [5] developed a similar two-dimensional mathematical model for interdigitated flow fields and studied the effects of the electrode thickness and the width of the shoulders of the gas flow field on the cell performance. Liu and Zhou [6] used a three-dimensional fuel cell model to study the effect of mass transfer enhancement with the interdigitated flow field. The effects of gas channel width, gas diffusion layer (GDL) thickness, and GDL porosity were also reported.

Experimental and modeling studies on the PEM fuel cell performance with interdigitated flow fields are very limited in literature, especially systematic experimental studies with different operation parameters. However such studies are very valuable for fuel cell developers to optimize fuel cell designs and operations. Besides, the recent upsurge in the efforts on fuel cell model development has created an urgent need for systematic experimental data on fuel cells with commercially available components. We therefore conducted systematic experiments on a PEM fuel cell

* Corresponding author.
E-mail address: hliu@miami.edu (H. Liu).

0378-7753/$ – see front matter © 2004 Elsevier B.V. All rights reserved.
doi:10.1016/j.jpowsour.2004.03.055

Nomenclature

ai_0^{ref}	reference exchange current density times area (A/m^3)
c	mole concentration of the gas mixture (mol/m^3)
c_{H^+}	proton mole concentration (mol/m^3)
c_p	specific heat at constant pressure (J/kg K)
D	diffusion coefficient (m^2/s)
E	fuel cell voltage (V)
E_0	open circuit potential (V)
F	Faraday constant (96,487 charge/mol)
i	current density (A/m^2)
$\mathbf{i}$	current density vector (A/m^2)
j	transfer current density (A/m^3)
k	thermal conductivity (W/m K)
k_p	permeability of the porous layer (m^2)
k_φ	electro-kinetic permeability (m^2)
L_{ct}	catalyst layer thickness (m)
p	pressure (Pa)
$r^{(2)}$	correction factor in momentum
R	universal gas constant (8.314 J/(mol K))
S_k	mass generation rate (mol/(m^3 s))
S_T	heat generation rate (W/m^3)
T	temperature (K)
u	velocity vector (m/s)
X	mole fraction
z_f	charge number

Greek symbols

ε	porosity
η	electrode overpotential (V)
μ	viscosity (kg/(m s))
ρ	density (kg/m^3)
σ	ionic conductivity (Ω^{-1} m^{-1})

Subscripts

a	anode
ave	average
c	cathode
ct	catalyst layer
k	kth component
m	membrane
eff	effective

Superscripts

ref	reference

with interdigitated flow fields to study the effects of various operation parameters. The membrane, catalyst, GDLs and collector plates used in this study are all commercially available. A three-dimensional mathematical model [6] was also used to simulate the fuel cell performance and compared with the experimental data.

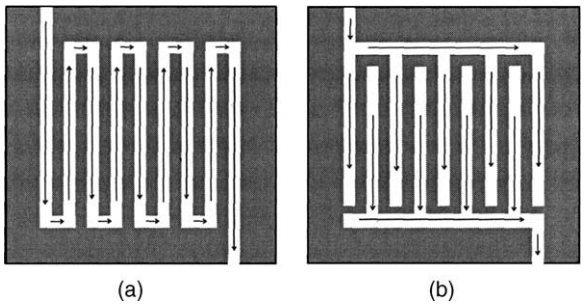

Fig. 1. Schematic illustrations of two different flow fields: (a) serpentine flow field; (b) interdigitated flow field.

2. Experimental

The fuel cell test station (FCTS) was manufactured by Fuel Cell Technologies, Inc. The test station can control the fuel cell temperature, humidification temperatures, backpressures and mass flow rates on both the anode and cathode sides. A schematic illustration of the FCTS is shown in Fig. 2. The cell and humidification temperatures are controlled by the OMEGA CN76000 thermocouple controllers. The reactant gases are humidified by passing through the humidifiers. Regulating the water temperature in the humidifiers controls the gas humidification. Two backpressure regulators at the outlets of the fuel cell are used to control the operating pressure. A computer with a Labview^{TM}-based software controls the MKS mass flow controllers. The amount of mass flow rate is set and read through the software. In each experiment, constant mass flow rates of reactant gases were used instead of constant stoichiometry to get complete polarization curves. The fuel cell polarization curves are obtained by controlling the HP6050 Electronic Load, which measures the cell output voltage and current.

A single PEM fuel cell with interdigitated flow fields was used for this experimental study. The membrane electrode assembly (MEA) was purchased from BCS Technology, Inc. The membrane used in the fuel cell is Nafion® 115. The catalyst is platinum with a loading of 0.4 mg/cm^2 per electrode. The gas diffusion layers are made of carbon fiber cloth with double micro-carbon layers. The MEA positioned between two graphite plates grooved with interdigitated gas channels is pressed between two gold-plated copper plates. The geometric parameters of the fuel cell are listed in Table 1.

Experiments with different delays between every two data points were carried out, since it is critical to select a proper

Table 1
Geometric parameters of the experimental fuel cell

Active area (m^2)	5.0×10^{-3}
Gas channel length (m)	6.34×10^{-2}
Gas channel width (m)	1.14×10^{-3}
Gas channel depth (m)	8.89×10^{-4}
Shoulder width (m)	8.08×10^{-4}
Gas diffusion layer thickness (m)	3.05×10^{-4}
Catalyst layer thickness (m)	7.62×10^{-5}
Membrane thickness (m)	1.27×10^{-4}

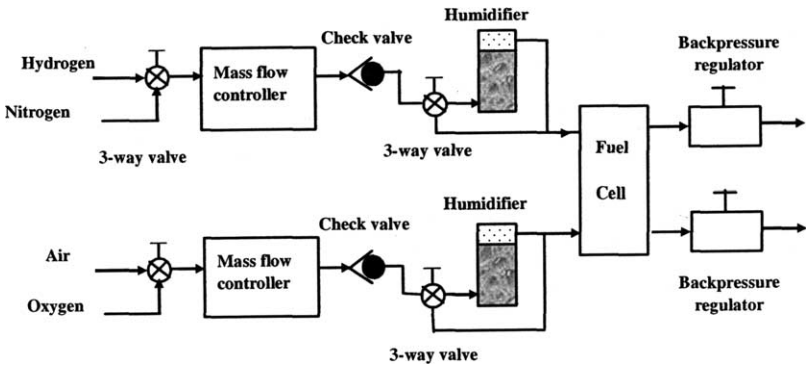

Fig. 2. The schematic illustration of the fuel cell test system.

delay to make sure that every point of voltage versus current is obtained after the fuel cell has reached a relatively steady state. After comparing the variation of the voltage and current with time, a delay of 200 s was selected.

3. Experimental results and discussion

3.1. Effect of fuel cell temperature

The effect of the cell temperature on the cell performance with the interdigitated flow fields has been studied. The experiments were carried out with the anode and cathode humidification temperatures of 70 °C. The anode and cathode backpressures were 1 atm. The hydrogen mass flow rate was 1200 sccm and the air mass flow rate was 2200 sccm. The experiments were carried out at different cell temperatures ranging from 40 to 90 °C, with an increment of 10 °C.

Fig. 3 shows that the cell performance improves as the cell temperature increases from 40 to 70 °C. When the cell temperatures are at 80 and 90 °C, which are higher than the humidification temperatures, the performance decreases drastically with the increase in cell temperature. The effect is clearly shown in Fig. 4, in which current density variations with the cell temperature at various different cell voltages are presented. When the cell temperature is below 70 °C, the current density increases with the increase in cell temperature. This is mainly due to the increase of exchange current density (reaction rate) with temperature. When the cell temperature is higher than the humidification temperature, the current density decreases sharply, which indicates that the membrane is dehydrated and the active catalyst surface area may also decrease. The effect of the cell temperature is more significant in the high current density region. At low current, the cell performance does not change much with the increase in the cell temperature.

From the above experimental results, it is seen that full hydration of the MEA is required for good fuel cell performances. To study the effect of operating temperature while minimizing the influence of humidification, another set of experiments with the humidification temperatures kept at 10 °C higher than the cell temperature were carried out.

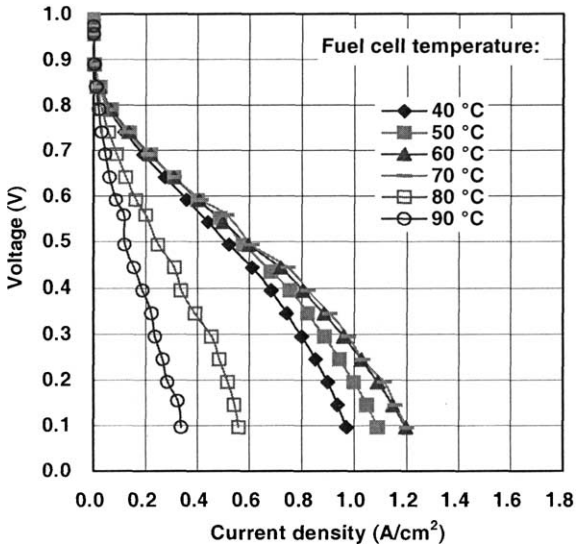

Fig. 3. Polarization curves for different fuel cell temperatures. Anode humidification temperature = 70 °C; cathode humidification temperature = 70 °C; anode backpressure = 1 atm; cathode backpressure = 1 atm; hydrogen flow rate = 1200 sccm; air flow rate = 2200 sccm.

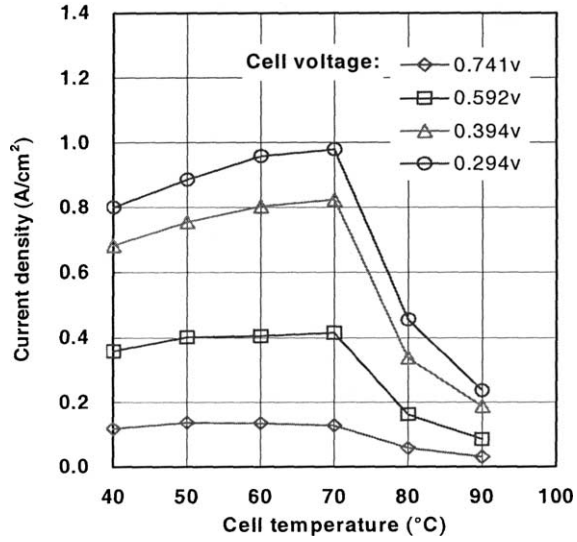

Fig. 4. Variation of current density with cell temperature at different cell voltages.

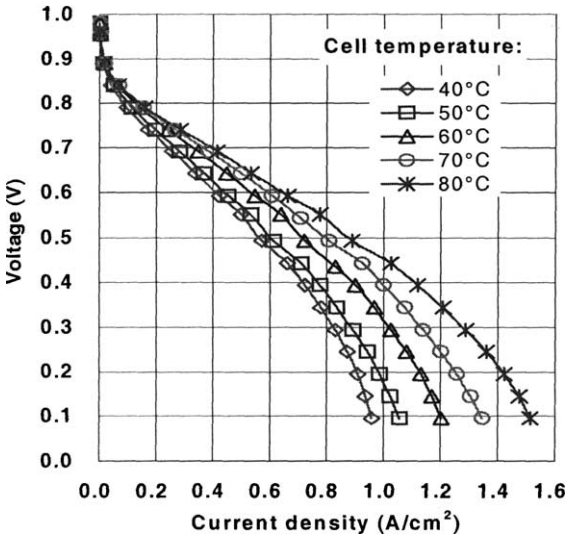

Fig. 5. Polarization curves for different fuel cell temperatures with the 10 °C higher humidification temperatures. Anode backpressure = 1 atm; cathode backpressure = 1 atm; hydrogen flow rate = 1200 sccm; air flow rate = 2200 sccm.

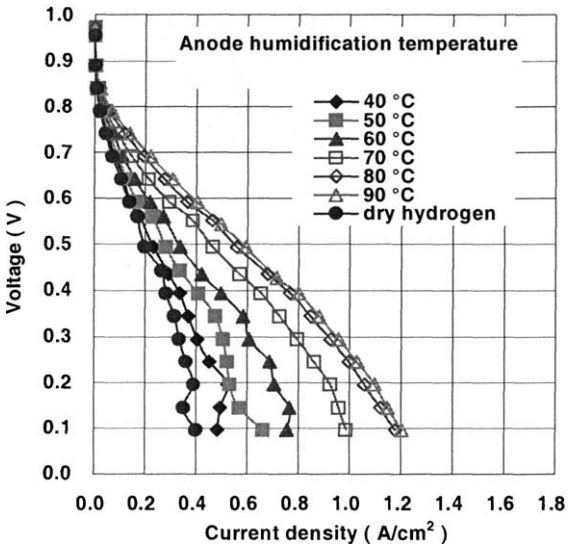

Fig. 7. Polarization curves for different anode humidification temperatures. Cell temperature = 70 °C; cathode humidification temperature = 70 °C; anode backpressure = 1 atm; cathode backpressure = 1 atm; hydrogen flow rate = 1200 sccm; air flow rate = 2200 sccm.

The cell temperature was changed from 40 to 80 °C with the interval of 10 °C. The experimental results of polarization curves are presented in Fig. 5. The cell performance improves with the increase of cell temperature, due to the increase of the membrane conductivity and the exchange current density. The relationship between the current density and cell temperature at different cell voltages is shown in Fig. 6. The current density changes approximately linearly with the cell temperature from 50 to 80 °C.

3.2. Effect of gas humidification

Two series of experiments were carried out to study the effect of humidification of the reactant gases on the cell performance with the interdigitated flow fields. One set of the experiments was conducted with different anode humidification temperatures while the cathode humidification temperature was kept at 70 °C. The other set of experiments was carried out with different cathode humidification temperatures and constant anode humidification temperature of 70 °C. For both sets of experiments, the cell temperature was maintained at 70 °C; the anode and cathode backpressures were 1 atm; the hydrogen mass flow rate was 1200 sccm and the air mass flow rate was 2200 sccm.

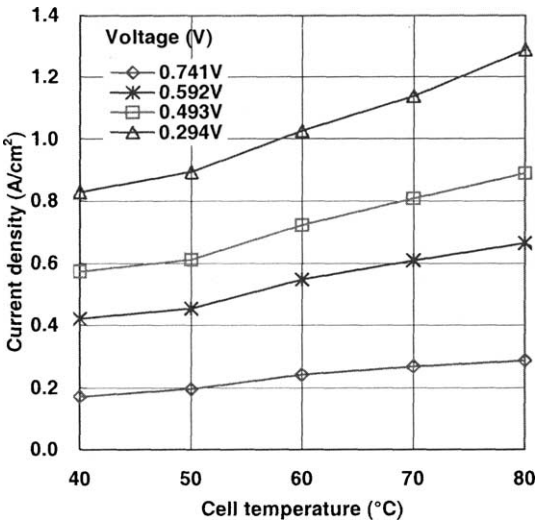

Fig. 6. Variation of current density with cell temperature at different cell voltages.

The polarization curves at different anode humidification temperatures are presented in Fig. 7. The polarization curve with dry hydrogen shows very low performance. The cell performance improves with the increase of the anode humidification temperature from 40 to 90 °C, with no significant difference between the cases of 80 and 90 °C. These results show that membrane is not fully hydrated even when the anode humidification temperature equals to the cell temperature, and there is no observable “flooding” even when the anode humidification temperature is as high as 90 °C. This improvement of the performance may be caused by the enhancement of water transport with the interdigitated flow field. The change of the current density with the anode humidification temperature at different voltages is presented in Fig. 8.

The experimental results with different cathode humidification temperatures are presented in Fig. 9. The change of the current density with cathode humidification temperature is shown in Fig. 10. The cell performs worst when dry air is used. The performance improves with the increase of the cathode humidification temperatures from 40 to 90 °C. Similar to the experimental results with different anode

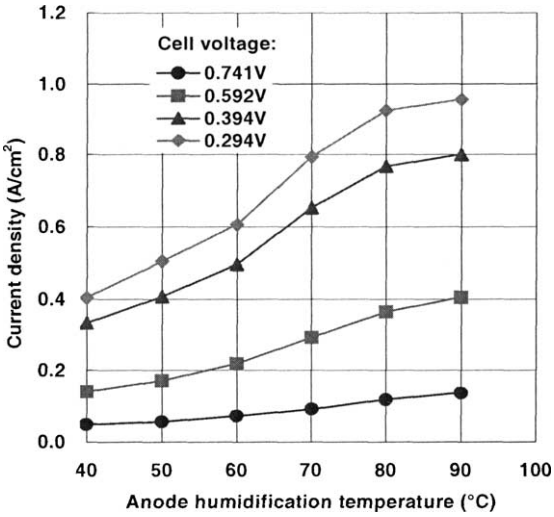

Fig. 8. Variation of current density with anode humidification temperature at different cell voltages.

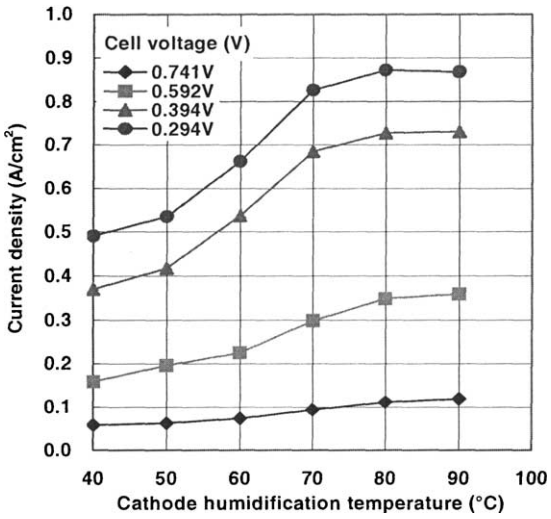

Fig. 10. Variation of current density with cathode humidification temperature at different cell voltages.

humidification temperatures, the cell performances with 80 and 90 °C cathode humidification temperatures are almost identical. This result is in contrast to the result obtained from a fuel cell with serpentine flow fields [1], which shows that the effect of cathode humidification temperature is insignificant. By comparing Fig. 7 with Fig. 9, it shows clearly that when the anode humidification temperature is higher than the cell temperature, the cell performances are better than that with the higher cathode humidification temperature than the cell temperature. The results indicate that no matter how much humidification is provided to the cathode side, if the anode humidification is not enough, the portion of the membrane close to the anode will not be fully hydrated. This is caused by water transfer from the anode to the cathode side due to electro-osmosis.

3.3. Effect of operation pressure

The experiments were carried out at different backpressures on both the anode and cathode sides from 1 to 3.72 atm. The cell and humidification temperatures at both the anode and cathode sides were 70 °C. The hydrogen mass flow rate was 1200 sccm and the air mass flow rate was 2200 sccm. The polarization curves are shown in Fig. 11. The cell performance increases with the increase of the backpressure because of the increase in the partial pressure of the reactant gases.

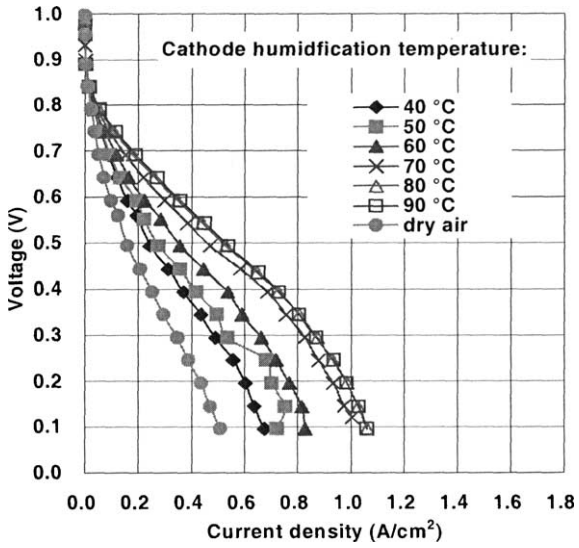

Fig. 9. Polarization curves for different cathode humidification temperatures. Cell temperature = 70 °C; anode humidification temperature = 70 °C; anode backpressure = 1 atm; cathode backpressure = 1 atm; hydrogen flow rate = 1200 sccm; air flow rate = 2200 sccm.

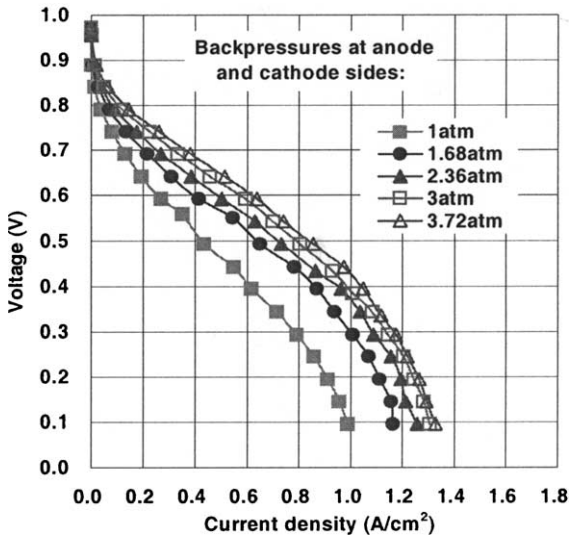

Fig. 11. Polarization curves for different backpressures. Cell temperature = 70 °C; anode humidification temperature = 70 °C; cathode humidification temperature = 70 °C; hydrogen flow rate = 1200 sccm; air flow rate = 2200 sccm.

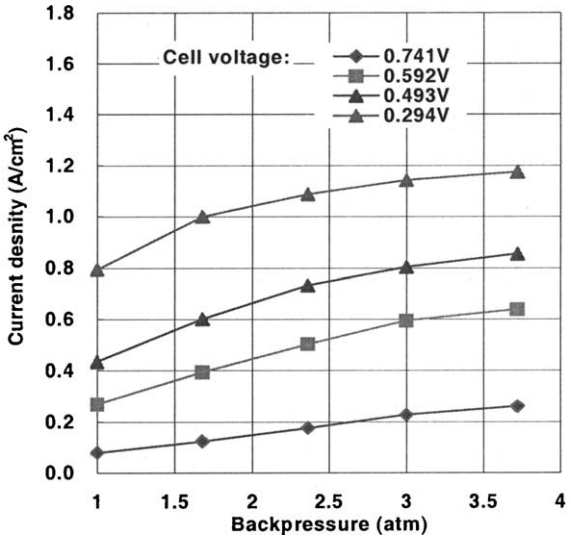

Fig. 12. Change in current density at different backpressures.

The change in current density under different cell voltages with various backpressures is shown in Fig. 12. The current density increases monotonously with the increase in backpressure. The open circuit potential and the exchange current density all increase with the increase in reactant partial pressure.

3.4. Effect of reactant gas flow rate

Experiments with different air mass flow rates ranging from 400 to 2200 sccm have been carried out at constant cell temperature of 70 °C. Anode and cathode humidification temperatures were 70 °C. The backpressures at both the anode and cathode sides were 1 atm. The anode flow rate was kept at 1200 sccm. Stoichiometric ratio of different cathode flow rates at some reference current densities are listed in Table 2. Fig. 13 shows that the cell performance increases when the cathode mass flow rate increases from 300 to 1200 sccm. The change of the current density with the hydrogen flow rate at different cell voltages is plotted in Fig. 14.

Table 2
Stoichiometric ratios at reference current densities of cathode flow rates

Cathode mass flow rate (sccm)	Reference current density (A/cm^2)	Stoichiometric ratio
400	0.4	1.21
500	0.5	1.21
600	0.5	1.45
800	0.5	1.93
1000	1	1.21
1200	1	1.45
1500	1	1.81
1800	1	2.17
2000	1	2.41
2200	1	2.65

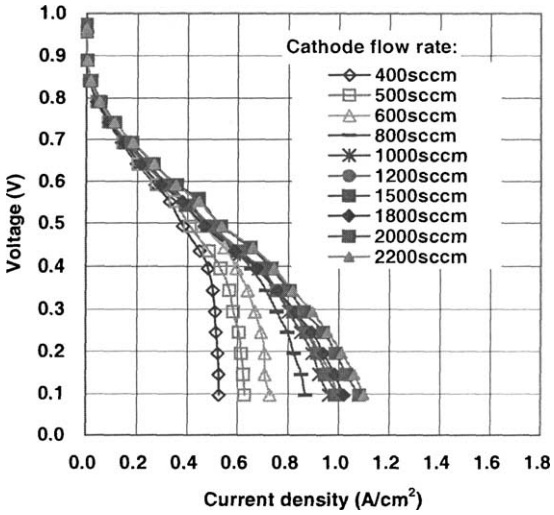

Fig. 13. Polarization curves for different air flow rates. Cell temperature = 70 °C; anode humidification temperature = 70 °C; cathode humidification temperature = 70 °C; anode backpressure = 1 atm; cathode backpressure = 1 atm; hydrogen flow rate = 1200 sccm.

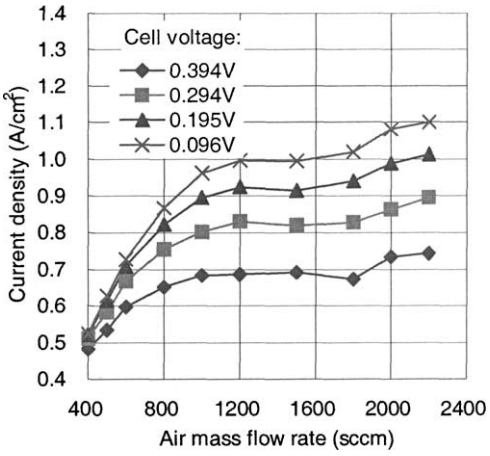

Fig. 14. Change in current density with different air mass flow rates.

4. Mathematical model

4.1. Model description

A three-dimensional mathematical model for PEM fuel cells with interdigitated flow fields was developed [7]. This three-dimensional model includes both the anode and cathode sides with their respective flow channels separated by the MEA. The schematic illustration of the geometric model of the half cell is shown in Fig. 15. The exit of the gas inlet channel and the entrance of the gas outlet channel are blocked. Governing equations of continuity, momentum, energy, and species concentrations of different components of a fuel cell, as well as the equations for phase potential in the membrane and the catalyst layer are coupled with chemical reaction kinetics by introducing various source terms.

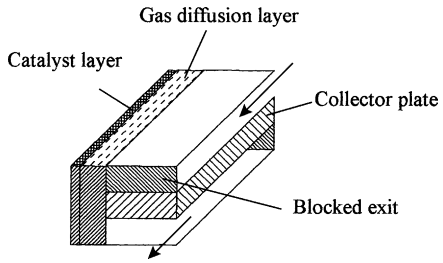

Fig. 15. Schematic illustration of the geometric model of a half cell.

The major governing equations are:
Continuity equation:

$$\nabla \cdot \rho \mathbf{u} = 0 \tag{1}$$

Momentum equation:

$$\rho \mathbf{u} \cdot (\nabla \mathbf{u}) = -\nabla p + \begin{cases} \mu \Delta \mathbf{u}, & \\ r^{(2)} \mu \Delta \mathbf{u} - \dfrac{\varepsilon \mu}{k_\mathrm{p}} \mathbf{u}, & \\ r^{(2)} \mu \Delta \mathbf{u} - \dfrac{\varepsilon \mu}{k_\mathrm{p}} \mathbf{u} - \dfrac{c_{\mathrm{H}^+} z_f F k_\phi}{k_\mathrm{p}} \cdot \dfrac{\mathbf{i}}{\sigma}, & \end{cases} \begin{matrix} \text{gas channel,} \\ \text{GDL,} \\ \text{catalyst layer and membrane} \end{matrix} \tag{2}$$

Energy equation:

$$\rho c_p \mathbf{u} \cdot (\nabla T) = k_\mathrm{eff} \Delta T + \begin{cases} 0, & \text{gas channel and diffusion layer,} \\ S_T, & \text{catalyst layer and membrane} \end{cases} \tag{3}$$

where the heat generation S_T is

$$S_T = \begin{cases} j\eta + \dfrac{i^2}{\sigma_\mathrm{ct}}, & \text{catalyst layer,} \\ \dfrac{i^2}{\sigma_\mathrm{m}}, & \text{membrane} \end{cases} \tag{4}$$

Species equation:

$$\mathbf{u} \cdot (\nabla X_k) = D_\mathrm{eff} \Delta X_k + \begin{cases} 0, & \text{gas channel and diffusion layer,} \\ \dfrac{S_k}{c}, & \text{catalyst layer} \end{cases} \tag{5}$$

At the cathode, the mass source terms for oxygen, water and protons are $j_\mathrm{c}/4F$, $-j_\mathrm{c}/2F$ and j_c/F, respectively. At the anode, the source terms for hydrogen molecules and protons are and respectively. $-j_\mathrm{a}/2F$, and j_c/F, respectively. j_a and j_c are the volumetric current densities at the anode and cathode, respectively, calculated from Butler–Volmer expression:

$$j_\mathrm{a} = (a i_0^\mathrm{ref})_\mathrm{a} \left(\frac{c_{\mathrm{H}_2}}{c_{\mathrm{H}_2}^\mathrm{ref}} \right)^{1/2} [\mathrm{e}^{(\alpha_\mathrm{a}^\mathrm{a} F/RT)\eta_\mathrm{a}} - \mathrm{e}^{-(\alpha_\mathrm{c}^\mathrm{a} F/RT)\eta_\mathrm{a}}] \tag{6}$$

$$j_\mathrm{c} = (a i_0^\mathrm{ref})_\mathrm{c} \left(\frac{c_{\mathrm{O}_2}}{c_{\mathrm{O}_2}^\mathrm{ref}} \right) [\mathrm{e}^{(\alpha_\mathrm{a}^\mathrm{c} F/RT)\eta_\mathrm{c}} - \mathrm{e}^{-(\alpha_\mathrm{c}^\mathrm{c} F/RT)\eta_\mathrm{c}}] \tag{7}$$

The parameters $r^{(2)}$, D_eff and k_eff are defined as [8]:

$$r^{(2)} = \frac{2.25(1-\varepsilon)^2}{\varepsilon^2} \tag{8}$$

$$D_\mathrm{eff} = \begin{cases} D_k, & \text{gas channel,} \\ D_k \varepsilon^{1.5}, & \text{porous media} \end{cases} \tag{9}$$

and

$$k_\mathrm{eff} = \begin{cases} k_\mathrm{f}, & \text{gas channel,} \\ -2k_\mathrm{s} + \dfrac{1}{(\varepsilon/(2k_\mathrm{s}+k_\mathrm{f})) + ((1-\varepsilon)/3k_\mathrm{s})}, & \text{porous media} \end{cases} \tag{10}$$

As $\mathbf{i} = -\sigma \nabla \eta$, the membrane phase potential satisfies:

$$\nabla \cdot (\sigma \nabla \eta) = \begin{cases} j_\mathrm{c}, & \text{cathode catalyst layer,} \\ 0, & \text{membrane,} \\ j_\mathrm{a}, & \text{anode catalyst layer} \end{cases} \tag{11}$$

The cell potential is given by

$$E = E_0 - |\eta_\mathrm{c}| - |\eta_\mathrm{a}| - \int_\mathrm{mem} \frac{i_\mathrm{ave}}{\sigma_\mathrm{m}} \mathrm{d}y \tag{12}$$

where E_0 is the open circuit voltage. In the simulation, the value of E_0 is determined from the experimental data.

4.2. Comparison of modeling results with the experimental data

Shown in Fig. 16 is the comparison of the polarization curves obtained by the three-dimensional model with experimental data at different operating fuel cell temperatures. Anode and cathode humidification temperature are both at 70 °C. The operating pressures are 1 atm on both the anode and cathode sides and flow rates are 1200 sccm on the anode side and 2200 sccm on the cathode side. It can be seen that the modeling results compare well with the experimental data.

Fig. 17 shows the comparison of the resulting polarization curves from the model with experimental data for different operating pressures. The fuel cell operating temperature and humidification temperatures of both the anode and cathode sides are 70 °C. The flow rates are 1200 sccm on the anode side and 2200 sccm on the cathode side.

It can be seen that the comparison is good at low and medium current densities. At high current densities, the

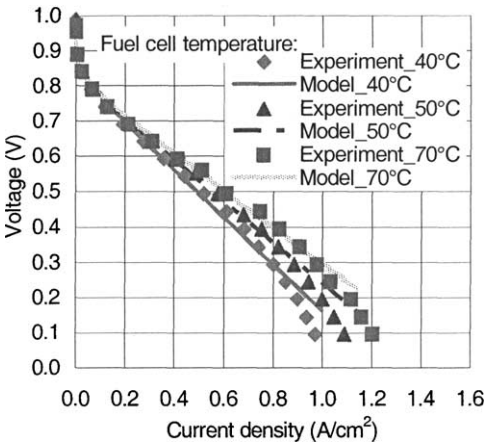

Fig. 16. Comparison of the modeling results and the experimental data for different fuel cell temperatures. Anode humidification temperature = 70 °C; cathode humidification temperature = 70 °C; anode backpressure = 1 atm; cathode backpressure = 1 atm; hydrogen flow rate = 1200 sccm; air flow rate = 2200 sccm.

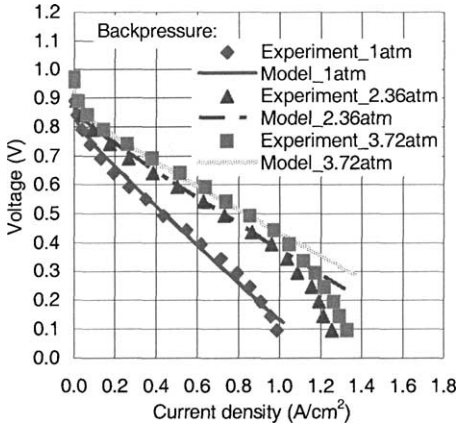

Fig. 17. Comparison of the modeling results and the experimental data for different backpressures. Cell temperature = 70 °C; anode humidification temperature = 70 °C; cathode humidification temperature = 70 °C; hydrogen flow rate = 1200 sccm; air flow rate = 2200 sccm.

difference between the modeling results and experimental data increases, and the model always over-predicts current density. At high current density region, the low current density of the experimental results may be caused by the presence of liquid water in the catalyst layers and the gas diffusion layer. Due to the presence of liquid water, the effective porosity of the gas diffusion layers and catalyst layers reduces, and the mass transfer resistance increases. Since the current model neglect the volume occupied by liquid water in the gas diffusion layers and catalyst layers, the increase of the mass transfer resistance effect cannot be considered.

5. Conclusions

In this work, the performance of a PEM fuel cell with interdigitated flow fields has been studied experimentally and numerically. Six sets of parametric experiments with different fuel cell temperatures, humidification temperatures, backpressures and mass flow rates have been performed. In addition to the polarization curves, the experimental data are also tabulated in the Appendix to facilitate future modeling comparisons. The following conclusions under the given experimental conditions are made:

1. When enough humidification is provided, the performance of the PEM fuel cell improves with the increase in fuel cell temperature. However, if not enough humidification is provided, the performance of the fuel cell deteriorates. This is due to the decrease of the membrane conductivity and possibly the reduction of active catalyst surface area.
2. Both anode and cathode humidification have significant effects on the performance of the PEM fuel cell with interdigitated flow fields, which is different from a fuel cell with serpentine flow fields [1]. With the increase in the anode and cathode humidification temperature, the cell performance improves until the humidification temperature is 20 °C higher than the cell temperature.
3. The performance of the fuel cell increases with the increase in operation pressure.
4. The modeling results show a good agreement with the experimental data, except in the high current density region.

Appendix A

Experimental data with different cell temperatures

V (V)	i (A/cm^2)					
	40 °C	50 °C	60 °C	70 °C	80 °C	90 °C
0.989	0.0002	0.0002	–	–	–	–
0.973	–	–	0.0002	0.0002	0.0002	0.0002
0.956	0.0006	0.0006	0.0006	0.0006	0.0002	0.0002
0.890	0.0053	0.0056	0.0049	0.0053	0.0036	0.0036
0.841	0.0226	0.0266	0.0239	0.0233	0.0132	0.0090

Appendix A (*Continued*)

V (V)	i (A/cm^2)					
	40 °C	50 °C	60 °C	70 °C	80 °C	90 °C
0.791	0.0602	0.0712	0.0672	0.0645	0.0329	0.0206
0.741	0.1192	0.1378	0.1364	0.1284	0.0579	0.0312
0.692	0.1931	0.2204	0.2194	0.2117	0.0898	0.0472
0.642	0.2750	0.3100	0.3103	0.3096	0.1248	0.0619
0.592	0.3589	0.4008	0.4045	0.4141	0.1634	0.0862
0.543	0.5044	0.4177	0.4981	0.5601	0.6816	0.1331
0.493	0.5197	0.5757	0.5957	0.6094	0.2487	0.1198
0.443	0.6670	0.5611	0.7189	0.7479	0.3123	0.1565
0.394	0.6820	0.7546	0.8035	0.8238	0.3376	0.1884
0.344	0.7412	0.8232	0.8854	0.9070	0.3912	0.2227
0.294	0.8005	0.8857	0.9590	0.9787	0.4551	0.2364
0.245	0.8527	0.9447	1.0272	1.0336	0.4828	0.2667
0.195	0.8998	0.9996	1.0912	1.1159	0.5174	0.2844
0.145	0.9374	1.0476	1.1475	1.1571	0.5408	0.3230
0.096	0.9716	1.0905	1.1984	1.2034	0.5590	0.3389

Anode humidification temperature = 70 °C; cathode humidification temperature = 70 °C; anode backpressure = 1 atm; cathode backpressure = 1 atm; hydrogen flow rate = 1200 sccm; air flow rate = 2200 sccm.

Experimental data with different fuel cell temperatures with the 10 °C higher humidification temperatures

V (V)	i (A/cm^2)					
	40 °C	50 °C	60 °C	70 °C	80 °C	90 °C
0.989	0.0002	–	–	–	–	–
0.981	–	0.0002	–	–	–	0.0002
0.973	–	–	0.0002	0.0002	–	–
0.956	0.0006	0.0002	0.0002	0.0002	0.0002	0.0002
0.890	0.0043	0.0046	0.0042	0.0043	0.0029	0.0046
0.841	0.0179	0.0210	0.0213	0.0216	0.0166	0.0210
0.791	0.0486	0.0575	0.0622	0.0656	0.0538	0.0575
0.741	0.0955	0.1128	0.1238	0.1328	0.1148	0.1128
0.692	0.1518	0.1800	0.1970	0.2127	0.1898	0.1800
0.642	0.2098	0.2500	0.2746	0.2960	0.2693	0.2500
0.592	0.2710	0.3206	0.3559	0.3829	0.3542	0.3206
0.559	0.3316	0.3892	0.4348	0.4512	0.4123	0.3892
0.493	0.3909	0.4584	0.5147	0.5534	0.5314	0.4584
0.443	0.4658	0.5461	0.6180	0.6626	0.6333	0.5461
0.394	0.5207	0.6060	0.6896	0.7392	0.7352	0.6060
0.344	0.5728	0.6646	0.7579	0.8135	0.8161	0.6646
0.294	0.6220	0.7175	0.8212	0.8830	0.8937	0.7175
0.245	0.6699	0.7705	0.8821	0.9500	0.9667	0.7705
0.195	0.7139	0.8191	0.9390	1.0116	1.0376	0.8191
0.145	0.7536	0.8641	0.9900	1.0649	1.0976	0.8641
0.096	0.7898	0.9054	1.0366	1.1142	1.1518	0.9054

Anode backpressure = 1 atm; cathode backpressure = 1 atm; hydrogen flow rate = 1200 sccm; air flow rate = 2200 sccm.

Experimental data with different anode humidification temperatures

V (V)	i (A/cm^2)						
	40 °C	50 °C	60 °C	70 °C	80 °C	90 °C	Dry hydrogen
0.973	0.0002	0.0002	0.0002	0.0002	0.0002	–	–
0.965	–	–	–	–	–	0.0002	–
0.956	0.0002	0.0002	0.0002	0.0002	0.0002	0.0002	0.0002
0.890	0.0023	0.0026	0.0029	0.0032	0.0042	0.0053	0.0016
0.841	0.0090	0.0099	0.0126	0.0153	0.0193	0.0235	0.0073
0.791	0.0246	0.0302	0.0345	0.0439	0.0579	0.0685	0.0216
0.741	0.0488	0.0562	0.0722	0.0915	0.1178	0.1364	0.0422
0.692	0.0796	0.0912	0.1104	0.1461	0.1927	0.2197	0.0695
0.642	0.1151	0.1262	0.1591	0.2121	0.2746	0.3080	0.1038
0.592	0.1398	0.1711	0.2191	0.2937	0.3643	0.4045	0.1378
0.559	0.1775	0.2290	0.2707	0.3671	0.4431	0.4673	0.1688
0.493	02327	0.2794	0.3366	0.4638	0.5580	0.5930	0.1964
0.435	0.2913	0.3438	0.4212	0.5704	0.6796	0.7001	0.2760
0.394	0.3343	0.4072	0.4964	0.6527	0.7682	0.8002	0.2797
0.344	0.3685	0.4761	0.5840	0.7262	0.8485	0.8807	0.3156
0.294	0.4046	0.5051	0.6066	0.7945	0.9261	0.9573	0.3326
0.245	0.4528	0.5211	0.6890	0.8628	0.9970	1.0313	0.3596
0.195	0.5230	0.5317	0.7059	0.9240	1.0578	1.0955	0.3892
0.145	0.4941	0.5687	0.7665	0.9567	1.1202	1.1478	0.3493
0.096	0.4834	0.6633	0.7553	0.9863	1.1771	1.2017	0.3986

Cell temperature = 70 °C; cathode humidification temperature = 70 °C; anode backpressure = 1 atm; cathode backpressure = 1 atm; hydrogen flow rate = 1200 sccm; air flow rate = 2200 sccm.

Experimental data with different cathode humidification temperatures

V (V)	i (A/cm^2)						
	40 °C	50 °C	60 °C	70 °C	80 °C	90 °C	Dry hydrogen
0.998	–	–	–	–	–	–	0.0002
0.989	0.0002	0.0002	–	–	–	–	–
0.973	–	–	0.0002	–	0.0002	0.0002	–
0.965	–	–	–	0.0002	–	–	–
0.956	0.0006	0.0006	0.0002	0.0002	0.0002	0.0002	0.0006
0.890	0.0043	0.0043	0.0036	0.0040	0.0036	0.0039	0.0043
0.841	0.0149	0.0153	0.0149	0.0156	0.0176	0.0193	0.0109
0.791	0.0338	0.0362	0.0389	0.0452	0.0532	0.0578	0.0220
0.741	0.0589	0.0629	0.0738	0.0942	0.1105	0.1185	0.0359
0.692	0.0895	0.0952	0.1191	0.1544	0.1821	0.1921	0.0522
0.642	0.1208	0.1328	0.1658	0.2207	0.2617	0.2716	0.0729
0.592	0.1588	0.1957	0.2244	0.3002	0.3489	0.3592	0.0979
0.559	0.1964	0.2166	0.2728	0.3580	0.4101	0.4209	0.1258
0.493	0.2450	0.2750	0.3576	0.4691	0.5297	0.5394	0.1594
0.443	0.3133	0.3572	0.4461	0.5962	0.6297	0.6359	0.2074
0.394	0.3709	0.4179	0.5368	0.6850	0.7269	0.7296	0.2534
0.344	0.4342	0.4955	0.5903	0.7559	0.8044	0.8042	0.2946
0.294	0.4904	0.5354	0.6620	0.8279	0.8728	0.8687	0.3480
0.245	0.5564	0.6819	0.7182	0.8774	0.9306	0.9340	0.3872
0.195	0.6027	0.7005	0.7665	0.9316	0.9859	0.9849	0.4359
0.145	0.6363	0.7525	0.8148	0.9749	1.0270	1.0283	0.4701
0.096	0.6746	0.7222	0.8275	1.0352	1.0622	1.0615	0.5090

Cell temperature = 70 °C; anode humidification temperature = 70 °C; anode backpressure = 1 atm; cathode backpressure = 1 atm; hydrogen flow rate = 1200 sccm; air flow rate = 2200 sccm.

Experimental data with different backpressures

V (V)	i (A/cm^2)				
	1 atm	1.68 atm	2.36 atm	3 atm	3.72 atm
0.973	–	–	0.0002	0.0002	0.0002
0.965	0.0002	0.0002	–	–	–
0.956	0.0002	0.0006	0.0006	0.0013	0.0013
0.890	0.0026	0.0052	0.0096	0.0136	0.0189
0.841	0.0136	0.0232	0.0375	0.0492	0.0655
0.791	0.0389	0.0632	0.0918	0.1192	0.1454
0.741	0.0795	0.1238	0.1751	0.2264	0.2604
0.692	0.1305	0.2030	0.2680	0.3343	0.3799
0.642	0.1934	0.2943	0.3853	0.4565	0.5154
0.592	0.2693	0.3939	0.5031	0.5941	0.6386
0.543	0.3656	0.5041	0.6310	0.6996	0.7399
0.493	0.4348	0.6007	0.7326	0.8031	0.8547
0.443	0.5484	0.7422	0.8460	0.9122	0.9730
0.394	0.6183	0.8404	0.9617	0.9945	1.0489
0.344	0.7156	0.9234	1.0376	1.0835	1.1080
0.294	0.7928	1.0016	1.0889	1.1434	1.1748
0.245	0.8567	1.0675	1.1562	1.2034	1.2181
0.195	0.9097	1.1055	1.1940	1.2434	1.2646
0.145	0.9570	1.1358	1.2131	1.2824	1.2937
0.096	0.9883	1.1705	1.2567	1.3047	1.3280

Cell temperature = 70 °C; anode humidification temperature = 70 °C; cathode humidification temperature = 70 °C; hydrogen flow rate = 1200 sccm; air flow rate = 2200 sccm.

Experimental data with different air mass flow rates

V (V)	i (A/cm^2)					
	400 sccm	600 sccm	800 sccm	1200 sccm	1800 sccm	2200 sccm
0.965	–	–	–	–	0.0002	0.0002
0.956	0.0002	0.0002	0.0002	0.0002	–	–
0.890	0.0026	0.0029	0.0029	0.0029	0.0026	0.0029
0.841	0.0132	0.0139	0.0149	0.0156	0.0142	0.0159
0.791	0.0408	0.0445	0.0452	0.0455	0.0422	0.0525
0741	0.0865	0.0945	0.0962	0.0965	0.0892	0.1121
0.692	0.1408	0.1548	0.1631	0.1615	0.1482	0.1864
0.642	0.1998	0.2273	0.2364	0.2303	0.2153	0.2693
0.592	0.2723	0.3103	0.3153	0.3159	0.2936	0.3546
0.551	0.3312	0.3809	0.3905	0.3956	0.3803	0.4458
0.493	0.3829	0.4575	0.4908	0.4968	0.4674	0.5361
0.435	0.4482	0.5610	0.5917	0.6113	0.5883	0.6798
0.394	0.4821	0.5960	0.6527	0.6859	0.6729	0.7435
0.344	0.5011	0.6403	0.7129	0.7528	0.7572	0.8188
0.294	0.5098	0.6672	0.7539	0.8302	0.8278	0.8957
0.245	0.5134	0.6916	0.7961	0.8797	0.8927	0.9563
0.195	0.5211	0.7076	0.8222	0.9247	0.9410	1.0126
0.145	0.5257	0.7076	0.8514	0.9690	0.9836	1.0642
0.096	0.5244	0.7275	0.8667	0.9970	1.0202	1.1005

Cell temperature = 70 °C; anode humidification temperature = 70 °C; cathode humidification temperature = 70 °C; anode backpressure = 1 atm; anode backpressure = 1 atm; hydrogen flow rate = 1200 sccm.

References

[1] L. Wang, A. Husar, T. Zhou, H. Liu, Int. J. Hydrogen Energy 28 (2003) 1263.
[2] T.V. Nguyen, J. Electrochem. Soc. 143 (1996) L103.
[3] D.L. Wood, J.S. Yi, T.V. Nguyen, Electrochim. Acta 43 (1998) 3795.
[4] A. Kazim, H. Liu, P. Forges, J. Appl. Electrochem. 29 (1999) 1409.
[5] J.S. Yi, T.V. Nguyen, J. Electrochem. Soc. 146 (1999) 38.
[6] H. Liu, T. Zhou, J. Enhanced Heat Transfer 10 (2003) 257.
[7] T. Zhou, H. Liu, Int. J. Trans. Phenomena 3 (2001) 177.
[8] G. Dagan, Flow and Transport in Porous Formations, Springer-Verlag, 1989.